Minimizing Stitching Errors for Large Area Laser Surface Processing

Moises Alberto Ortega Delgado[a,b], Andrés Fabián Lasagni [a,b]

aFraunhofer-Institut für Werkstoff- und Strahltechnik IWS, Winterbergstr. 28, 01277 Dresden, Germany

bTechnische Universität Dresden, Institut für Fertigungstechnik, George-Bähr-Str. 3c 01069 Dresden, Germany

Direct laser writing is a well-known method for fabricating features in the micrometer scale on a large variety of materials. Several efforts for increasing the working field of a common direct-writing system have been made in the past. Basically, an improvement of the precision of used devices and the implementation of correction algorithms lead to achieve an acceptable accuracy over the complete working field. However, stitching strategies are needed to increase the working area as well as the precision. In this work, a procedure to facilitate the reduction of stitching deviations of a common direct-writing device for large areas has been developed. Using a novel vision system, deviations of the structures inside the working field are measured. Subsequently, different algorithms are used for reducing these stitching deviations. Preliminary results for a conventional laser micromachining device are presented here. Deviations were reduced between ~30% and ~80%.

1. Introduction

Laser micromachining of materials is nowadays an essential technique for different research and manufacturing areas. Different processes, laser sources, and systems make laser micromachining an adaptable method in diverse scientific areas. The direct laser writing technique has been very important since the development of the laser for adding, modifying or subtracting material used for many different applications [1]. Laser processing for large areas, commonly using excimer lasers, have been studied and developed due to the importance of large-scale applications [3, 4]. However galvanometer laser machining, in which the laser beam is positioned on a dynamic working field by means of two mirrors mounted in galvanometers also increased its importance for large areas in the last decades. Besides all the advantages of this method, like high resolution, repeatability and high processing velocity, there is an important restriction, which is a limited working area.

For processing larger working fields, the substrate is mounted on a coordinates table and sub-working fields are defined. The overall accuracy and finishing of the processing are directly influenced mainly by the accuracy of the scanner system, the coordinate´s table as well as by optical and mechanical distortions. Typically, an extra phase named "stitching" must be accomplished to correct deviations that come out between two different sub-working fields. For specific applications a compromise among accuracy, velocity and the above mentioned deviations can be reached. This can lead however, to increased costs and quality control phases.

In this work, a new strategy for allowing the reduction of stitching deviations of a common direct-writing device for large areas has been developed. Using an innovative vision system, deviations of the structures inside the working field are analyzed. This vision system is constituted of divergent and diffusive optics mounted on a linear axis for coupling and decoupling the optics for measuring and processing purposes (see Fig. 1). Afterwards different algorithms are used for reducing stitching deviations. In order to prove the advantages of this strategy, two approaches are presented in this work: an average correction and an individual correction.
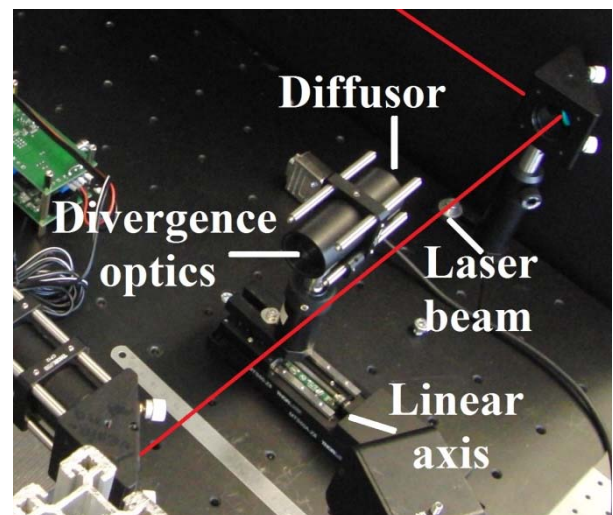
Fig. 1. Close up of the vision system device.

1.1 Inherent distortions in galvanometer laser systems

When galvanometer mirrors rotate at a constant velocity, the variation of the rotation angle θ of the mirror is constant during time. However, the relationship between rotation and position of the laser spot over the working plane

for each axis is not linear. The position over the working field as function of the rotation angle can be described by:

$$y = f_l \cdot \tan\theta \qquad (1)$$

where f_l is the focal length of the lens, y the position over the working field [2]. It is observed that the position of the spot changes proportionally to the tangent of the angle. Moreover, the position of the focal point´s plane does not remain constant causing the image in the working area to blur. By using flat field objectives, commonly called f-theta lenses, for focusing the laser beam it is possible to scan over a complete working area maintaining both the focal point´s plane and scanning velocity constant. In the last case, the position over the working field is approximated by [2]:

$$y = f_l \cdot \theta \qquad (2)$$

A disadvantage of using f-theta lenses is the introduction of different distortions, commonly known as geometrical deviations. These deviations do not cause the image to blur, but misshape. There are mainly three different geometrical deformations which are used to describe how the working field of a laser scanning system is deformed: (a) pillow-shape deformation, (b) barrel-shape deformation and (c) pillow-barrel-shape deformation (see Fig. 2) [6].
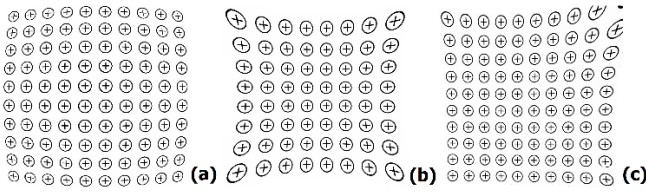
Fig. 2. Inherent and random deviations of galvanometer scanning systems: (a) Pillow shape deviation, (b) Barrel shape deviation and (c) pillow-barrel-shape deformation.

1.2 Mechanical distortions

Mechanical distortions are presented basically as developing errors and mounting errors [5]. They cause the laser beam to drift. Commonly this drift occurs because of misalignments of the scanner system or the laser beam itself.

Thermal effects are also a type of mechanical influenced deviation, since the position of the laser spot changes due to the change of temperature in the optics and mechanics [6]. Mechanical deviations and other non-systematic deviations cause the working field to deform in a non-symmetric way [7].

1.3 Reduction of distortions in the working field

Many compensating techniques have been used in the past in order to reduce inherent distortions for laser scanning systems [5-7]. In such techniques, the scanning system field is partitioned into a grid of n by n elements. A multi-variate interpolation method, commonly bilinear interpolation or bicubic interpolation, is used for finding the corresponding scanning points. It is assumed that the value of a function $f(x,y)$ (corresponding to the angles of the scanners X and Y) in at least four controlling points (lattice points), $CP_{0,0}$, $CP_{0,1}$, $CP_{1,0}$ and $CP_{1,1}$ is known [5] (see Fig.3).

Supposing then that the value of an unknown function (angles of X and Y scanners) $P_u = f(x,y)$ at a point (x,y), which is not a lattice point, has to be found.
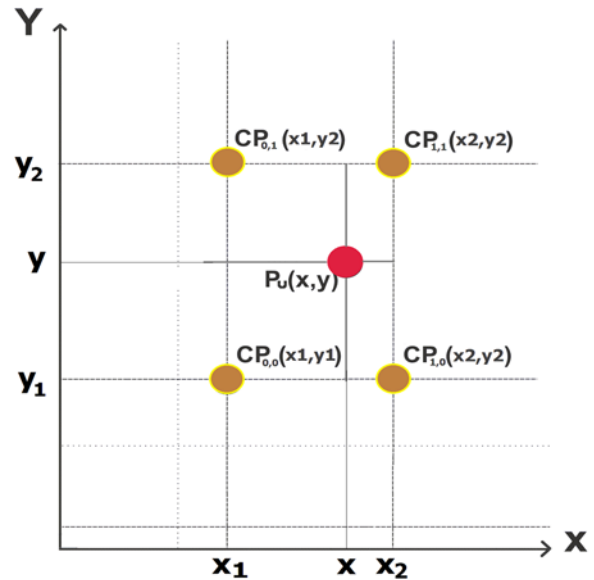
Fig. 3. Distribution of known controlling points for approximating the value of an unknown function $P_u(x,y)$ using four controlling points $CP_{n,n}$.

In order to find an approximated solution to the unknown function P_u, linear interpolations are calculated over each direction. The order of these interpolations yields the same results. For convention, the X direction ($f(x,y_1)$ and $f(x,y_2)$) is selected as initial direction:

$$f(x,y_1) = \frac{x_2 - x}{x_2 - x_1} f(CP_{0,0}) + \frac{x - x_1}{x_2 - x_1} f(CP_{1,0}) \qquad (3)$$

$$f(x,y_2) = \frac{x_2 - x}{x_2 - x_1} f(CP_{0,1}) + \frac{x - x_1}{x_2 - x_1} f(CP_{1,1}) \qquad (4)$$

Afterwards an interpolating in Y direction is made for finding the approximation of the unknown function:

$$P_u = f(x,y) = \frac{y_2 - y}{y_2 - y_1} f(x,y_1) + \frac{y - y_1}{y_2 - y_1} f(x,y_2) \qquad (5)$$

$$f(x,y) = \frac{y_2 - y}{y_2 - y_1}\left(\frac{x_2 - x}{x_2 - x_1} f(CP_{0,0}) + \frac{x - x_1}{x_2 - x_1} f(CP_{1,0}) \right)$$
$$+ \frac{y - y_1}{y_2 - y_1}\left(\frac{x_2 - x}{x_2 - x_1} f(CP_{0,1}) \right.$$
$$\left. + \frac{x - x_1}{x_2 - x_1} f(CP_{1,1}) \right) \qquad (6)$$

The accuracy of these algorithms depends on the accuracy and number of controlling points. A reduced number of controlling points lead to a poor distortion correction. On the other hand, if the number of controlling points is too large, the real-time capacity of the system is negatively influenced. The correction map is calculated theoretically assuming basic characteristics of f-theta lens, working field size and scanning angles and it is improved by measuring methods. Higher order polynomial functions or different curve fitting methods can also be used for approximating the error function [5-7]. Better designs, temperature control systems and intelligent self-adjusting mirrors are also some possibilities for increasing mechanical accuracy.

1.4 Monitoring devices in laser systems

CCD and CMOS cameras have been used in laser systems in order to analyze welding processes [8-11]. Commonly, these coaxially monitoring systems analyze the properties of welding keyhole and adjust variables like scanning velocity and laser power in order to maintain the same welding characteristics over the complete working task. Coaxially coupled devices have been also used for measuring the position (and applying required position corrections) of certain features [12, 13]. These devices work essentially in a similar way. One important condition is that the working wavelength of the illumination device and the camera are different to the one of the processing laser. This is necessary to protect the camera from the laser source. To do so, dichroic mirrors are introduced in the laser beam paths. In order to reduce the reflected power, neutral density filters are also built-in.

2. Strategy for increasing machining surface with minimized stitching errors

During this work, a new strategy for increasing machining surface was developed and tested. The strategy is based on the analysis of microstructures in the working field, the construction of an error vector and the calculation of new machining coordinates. In sum, the deviations presented between two different adjacent sub-working fields (stitching errors) are reduced and in some cases eliminated.

2.1 Development of a large area vision system

For analyzing microstructures in the working field and reducing deviations presented between two adjacent sub-working fields, a specific vision device was built. This device was used to analyze and compare target and real machining coordinates. Figure 4 shows a schematic representation of the system. An innovative component for illuminating the working field using the processing laser is included (also seen in Fig. 1). This is mounted on a linear translation stage for measuring and processing phases. The illumination optics was designed using AR-coated concave lenses (-50 mm, -75 mm and -100 mm) and AR-coated diffusers (600 Grit and 1500 Grit) in order to reduce the spatial and temporal coherence of the laser beam. This improves image quality. It also comprises neutral density filters for reducing laser intensity for protecting the camera.

An AR-coated beam splitter (10-90 split ratio) is used to reflect the light from the working field to the camera. When the illumination component is coupled, the illumination spot diameter is approximately 1-2 mm. Contrary to that, when the illumination component is decoupled and laser parameters are selected with minimal peak power, the laser beam is used as a pointer laser. This pointer improves and facilitates the recognition of specific points over the working field. Furthermore, external illumination approaches are also applied with the intention of improving image quality. For this approach, the same wavelength was used for both, the processing laser and the illumination laser. Using the same wavelength is possible to avoid an additional correction mapping due to chromatic aberration of the f-theta lens.
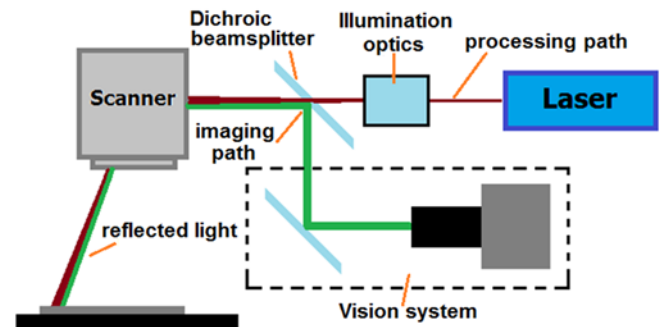
Fig. 4. General representation of the proposed correction approach for reducing stitching errors. Red color represents the processing path. Green color represents the path of reflected light.

2.2 Correction strategy

The strategy used in this work to reduce stitching is divided in five main steps:

i. **Preprocessing stage:** firstly, initial configuration for controller, scanner, camera and marking software are loaded. The working field is divided in m sub-fields $SF_{1,2,m}$ (Fig. 5 (a)). Each sub-field contains different structures to be machined. A n number of structures located between two sub-fields in an area defined as "common analysis area" (Fig. 5 (a)) are defined in a vector space denoted as F_m. In this area are found a n number of control points (called "target critical points"). The "target critical points" $C_{pT1} = (x_{T1}, y_{T1})$, $C_{pT2} = (x_{T2}, y_{T2})$, ... $C_{pTn} = (x_{Tn}, y_{Tn})$ are defined using the end points of the microstructures themselves as shown in Fig. 5 (b). The critical points are then used for constructing a transformation matrix and calculating a corrected vector space of n elements $F'_{m+1,n}$.

ii. **Processing of sub-field SF_1.:** with help of processing software, pilot laser and coordinate's table, the initial coordinates of the sub-working field SF_1 are found and the corresponding microstructures are processed. This allows having a global coordinates system, which will be used as principal reference point.

iii. **Analysis of critical points:** the working piece is then positioned at the sub-working field SF_{m+1}. With help of the scanner and the coaxially coupled vision system, the relative coordinates x_{Mn}, y_{Mn} of every "measured critical point" ($CP_{M1}, CP_{M2}, ... CP_{Mn}$) are searched in the "common analysis area" and compared with its corresponding target critical point ($CP_{Tn} = (x_{Tn}, y_{Tn})$) as shown in Fig. 5 (b). The measured deviation of every critical point is saved in an error vector $\vec{E}$, shown in equation 7.
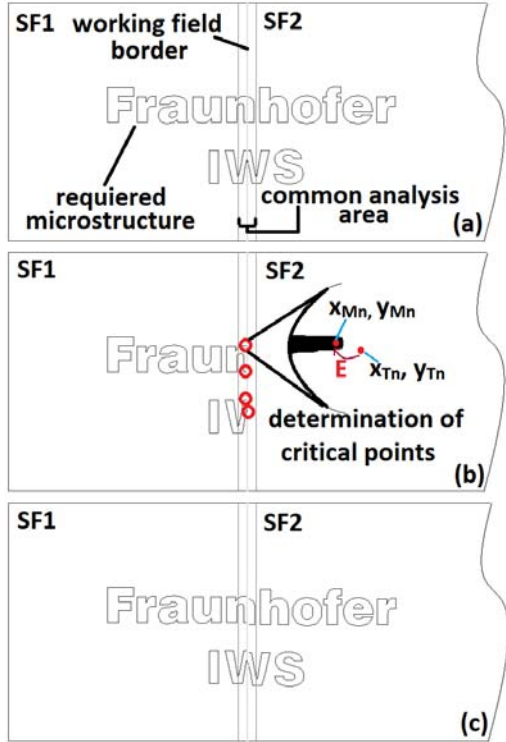
Fig. 5. Pre-analysis of microstructures. (a) Definition of microstructure, sub-working fields and common analysis area. (b) analysis of critical points. (c) Processing of new sub-field F_{m+1}.

$$\vec{E} = [E_x \quad E_y] = \begin{bmatrix} e_{x1} & e_{y1} \\ e_{x2} & e_{y1} \\ \vdots & \vdots \\ e_{xn} & e_{yn} \end{bmatrix} =$$
$$\begin{bmatrix} x_{M1} - x_{T1} & y_{M1} - y_{T1} \\ x_{M2} - x_{T2} & y_{M2} - y_{T2} \\ \vdots & \vdots \\ x_{Mn} - x_{Tn} & y_{Mn} - y_{Tn} \end{bmatrix} \quad (7)$$

Were E_x corresponds to the deviation in direction X and E_y correspongs to the deviation in direction Y.

This vector is used for constructing a transformation matrix T. The corresponding corrected vector space F'_{m+1} in the sub-working field SF_{m+1} is calculated as follows:

$$F'_{m+1,n} = T(E)F_{m+1,n} \quad (8)$$

iv. **Processing sub-field:** after new structures F'_m are calculated, the subsequent sub-field SF_{m+1} is processed (see Fig. 5 (c)). Steps 3 to 4 are repeated until the complete working field is finished.

v. **Actualization of correction table and evaluation of results:** the correction table is actualized using the information contained in the error vector $\vec{E}$. Finally, resulting microstructures are analyzed with optical microscopy. The measured deviations and new correction data can be saved in to the laser scanning system in order to improve relative precision.

In this work, two correction methods (average correction and individual correction) were analyzed. The corresponding matrices are calculated as follows:

for the average correction, a mean value of each column vector contained in the error vector $\vec{E}$ is calculated and applied to the microstructures of the subsequent sub-working field:

$$T_{am}(\vec{E}) = [E_{amx} \quad E_{amy}]$$
$$= \left[\frac{1}{n}\sum_{i=1}^{n} e_{xi} \quad \frac{1}{n}\sum_{i=1}^{n} e_{yi} \right], \quad (9)$$

for $i = 1:n$ yield:

$$F'_{m+1,i} = \begin{bmatrix} 1 & 0 & 0 & E_x \\ 0 & 1 & 0 & E_y \\ 0 & 0 & 1 & 0 \\ 0 & 0 & 0 & 1 \end{bmatrix} \begin{bmatrix} F_{mx+1,i} \\ F_{my+1,i} \\ 0 \\ 1 \end{bmatrix}$$
$$= \begin{bmatrix} F_{mx+1,i} + E_{amx} \\ F_{my+1,i} + E_{amy} \\ 0 \\ 1 \end{bmatrix}. \quad (10)$$

for the individual correction, every structure will be approximated by applying a transformation that relates a unique error vector for each structure:

$$T_{in}(\vec{E}) = [E_{inx} \quad E_{iny}] = \begin{bmatrix} e_{x1} & e_{y1} \\ e_{x2} & e_{y1} \\ \vdots & \vdots \\ e_{xn} & e_{yn} \end{bmatrix}, \quad (11)$$

for $i = 1:n$ yield:

$$F'_{m+1,i} = \begin{bmatrix} 1 & 0 & 0 & e_{xi} \\ 0 & 1 & 0 & e_{yi} \\ 0 & 0 & 1 & 0 \\ 0 & 0 & 0 & 1 \end{bmatrix} \begin{bmatrix} F_{mx+1,i} \\ F_{my+1,i} \\ 0 \\ 1 \end{bmatrix}$$
$$= \begin{bmatrix} F_{mx+1,i} + e_{xi} \\ F_{my+1,i} + e_{yi} \\ 0 \\ 1 \end{bmatrix}. \quad (12)$$

3. Experimental set-up

A pulsed fiber laser from Multiwave Photonics with a maximum power of 20 W was used. The laser emits at a center wavelength of 1064 nm with peak powers near to 15 kW. It is equipped with a collimator which offers a raw beam of 7 mm. Pulse widths in the range of 10 ns to 200 ns

with pulse repetition frequencies from single shot to 500 kHz can be selected [14]. A Miniscan-7 scanner from Raylase AG was used for this work. It has an aperture of 7 mm, resolution of 12 µrad and repeatability of 2 µrad (RMS) [15]. A standard f-theta lens (S4LFT0162/126 from SILL Optics) was selected as focusing optics. The f-theta optics is a lens made of optical glass with standard coating for 1064 nm. With a focal length of 160.1 mm and working distance of 180.1 mm [16], the optics allows a scanning area of approximately 100 mm x 100 mm. The reached spot size is 85 µm. A positioning system, consisting in 3 linear stages (PMT-160-DC-300-R from Feinmess Dresden GmbH) with 300 mm travel and accuracy of 20µm [17] was utilized. The system was controlled with a 4-axis Galil Ethernet/RS232 DMC2143 amplifying unit. In Fig. 6, the experimental set-up is depicted. For the vision system a UI-6140SE-M-GL CCD monochromatic camera from IDS Imaging Systems was used.
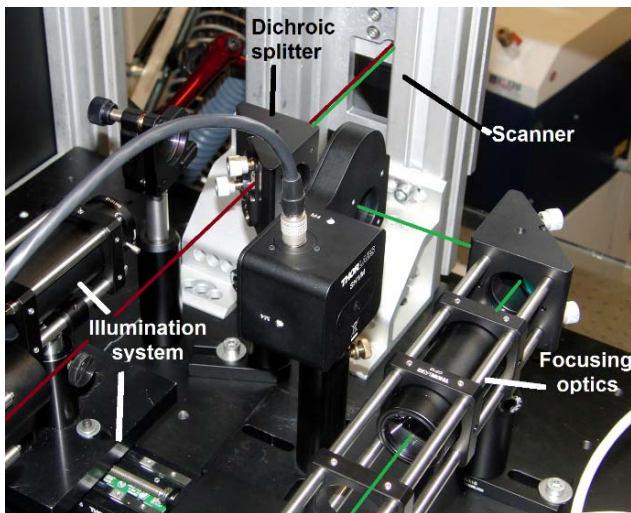
Fig. 6. Experimental set-up.

4. Results and Discussion

Two mapping functions were selected for the aim of this paper:

i. An average error vector is computed and a position transformation takes place using the coordinates table.

ii. An individual position correction for each microstructure is applied.

Series of experiments were prepared in order to test the functionality of the proposed strategy. The laser scanning system was corrected with a standard correction table and the positioning system´s controller tuned with Ziegler-Nichols closed-loop tuning method. An arrangement of parallel lines between two sub-fields at the upper and bottom side are desired, see Fig. 7(a).
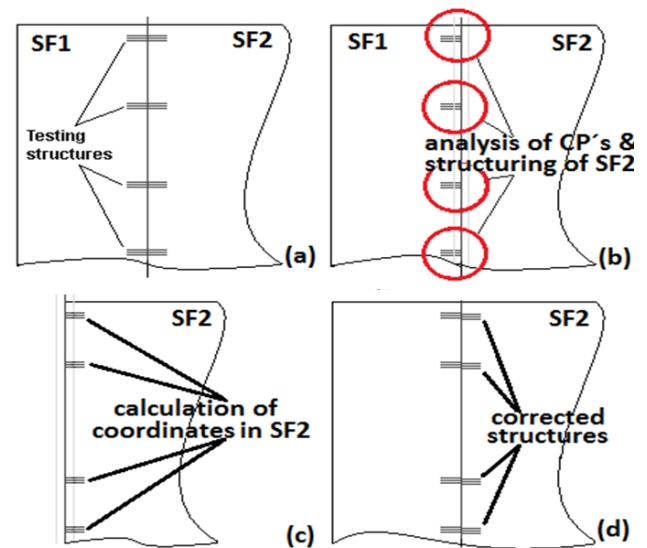
Fig. 7. Representation of initial experiments. An arrangement of parallel lines between two sub-fields is defined (a). The sub-working field SF1 is processed and the critical points analyzed (b). New coordinates in sub-working field SF2 are calculated (c) and subsequently processed (d).

Each sub-field has a dimension of 60 mm x 60 mm. The scanning velocity was 1800 mm/s and the repetition rate was 50 kHz. The used pulse length was 100 ns. The initial arrangement of parallel lines of the first sub-field SF_1 were programmed and scanned, see Fig. 7(b). After that, the origin of the next sub-field SF_2 was found (60 mm translation) and depending on the used function, either no correction or a position correction was calculated (see Fig. 7(c)). Finally, the next arrangement of parallel lines of the second sub-field SF_2 was programmed applying the corresponding mapping function and afterward scanned.

The maximum average deviation was obtained by the no-correction method for $Y - axis$ (Table 2). It exhibits a RMS value of ~55 µm. The minimum average deviation was obtained by the individual correction method for $X - axis$ (Table 1). It exhibits a value of ~10.4 µm. The feasibility of these methods was evaluated by observing the tendency for the deviations approaching to zero. For X axis, the average error improved from -14 µm for no-correction approach to -3.6 µm for the average correction approach and to -1.3 µm for individual approach (Table 1). For Y axis, the average error improved from 46.4 µm for no-correction approach to -18.4 µm for the average correction approach and to -11.5 µm for individual approach (Table 2).

By further analyzing the obtained information (Tables 1 and 2), it was observed that the measured data for the average correction approach and the individual correction approach (for Y axis) is negative in most of the cases. That means that there exists always an overlap between the stitched structures and only a few percentage of the structures remains disjointed. Moreover, the mean value tends to approach the zero axis, which means that there is a tendency for the deviations to be reduced.

Table 1. Selection of representative measured deviation for a series of experiments for no-correction approach, average correction approach and individual correction approach for X-axis.

No-correction tests	Average correction tests	Individual correction tests
Deviations in X direction [μm]	Deviations in X direction [μm]	Deviations in X direction [μm]
-17.0	-15.5	16.0
-17.8	6.0	7.0
-18.1	-6.5	3.5
-10.5	-8.5	1.5
-11.7	13.3	0.5
-4.4	11.4	7.5
-8.0	4.9	-7.5
-12.0	-8.3	-2.3
-15.7	-10.7	-9.1
-18.2	6.1	-4.7
-22.3	-8.8	3.3
-23.0	-27.5	-15.0
Mean error		
-14.9	-3.7	0.1
RMS		
15.8	12.2	8.1
σ		
5.6	12.1	8.4

Table 2. Selection of representative measured deviation for a series of experiments for no-correction approach, average correction approach and individual correction approach for Y-axis.

No-correction tests	Average correction tests	Individual correction tests
Deviations in Y direction [μm]	Deviations in Y direction [μm]	Deviations in Y direction [μm]
67.8	-11.2	-7.0
65.0	-15.0	-15.0
54.6	-13.1	-7.5
54.5	-11.2	-13.0
-47.0	-22.0	-7.5
43.0	-45.0	-5.6
28.0	-13.1	-13.1
47.0	-45.1	-18.9
56.4	-26.3	-13.2
47.0	-16.9	-15.0
60.2	-9.4	-8.0
80.9	7.5	-15.0
Mean error		
46.5	-18.4	-11.6
RMS		
55.8	23.2	12.3
σ		
32.3	14.8	4.2
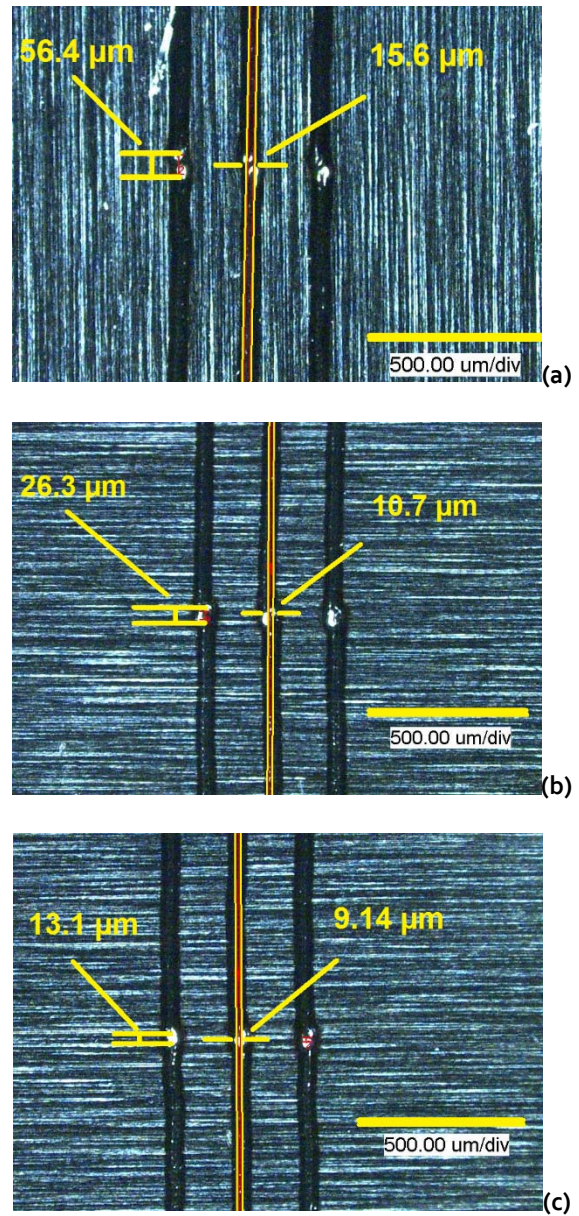
Fig. 8. Examples of structured substrates for the no-corrected approach (a), average correction approach (b) and individual correction approach (c).

In Fig. 8, three optical microscope images are shown, representing an example of the results without correction (Fig. 8a), after applying average correction (Fig. 8b) and individual correction approaches (Fig. 8c). For the uncorrected approach a deviation of 15.6 μm between structures in X direction and a deviation of 56.4 μm between the structures in Y direction were measured. For the average approach a deviation of 10.7 μm between structures in X direction and a deviation of 26.3 μm between the structures in Y direction were measured. These values correspond for this example to an improvement of ~31% and ~53% for X and Y directions respectively. Finally, for the individual approach a deviation of 9.14 μm between structures in X direction and a deviation of 13.1 μm between the structures in Y direction were measured. These values correspond for this example to an improvement of ~42% and ~76% for X and Y directions respectively compared with the uncorrected approach.

5. Conclusions and Outlook

The deviations reduction of the average correction approach depends directly on the inherent deviations of the optical system and the illumination homogeneity. In order for this method to have a positive effect by reducing deviations, the correction table of the galvanometer scanning system had to be already quite precise. The average improvement using this method for X-axis was about 16% and for Y-axis 60%. The method tends to be more effective if the detected average error is directly influenced by a difference of scales between coordinates systems or an offset difference between coordinates systems.

The individual correction method presents better results. The precision of the coordinates table of the galvanometer scanning system was less determining for the individual correction approach to show improvements since independent corrections for each structure were performed. The average improvement using this method for X-axis was about 48% and for Y-axis 77%. The method tends to be more effective if the structures to be corrected are open-paths structures, which means that corrected structures are not associated each other.

The possibility of combining both methods for reducing inherent deviations of a galvanometer scanning system can be further investigated. The possibility of applying a mean correction and subsequently individual corrections may have a positive influence for the final correction. Different galvanometer scanning systems can also be object of study implementing such correction methods.

Minimizing stitching errors for large area processing using the proposed approach presents different advantages. The reduction of the overall stitching deviations was assured using conventional scanning and positioning devices. Important to mention is that the accuracy of the used positioning device is ±20 µm. Even though, with the implementation of this method the stitching transitions were considerably improved. Deviations of ~5µm were measured, thus the deviations depend on the device with improved accuracy. The effects of the inherent deviations of the galvanometer scanning system were reduced. Implementing the given approach is much more cost-effective than coupling more accurate (and cost-intensive) devices.

Acknowledgment

References

[1] Craig B. Arnold, A. Piqué and A. Chimmalgi: Laser direct-write processing, MRS bulletin 32, (2007) 9.

[2] R.E. Fischer and B. Tadic-Galeb: Optical System Design, McGraw-Hill, New York (2000).

[3] A. Holmes, J. Pedder: Laser micromachining in 3D and large area applications, The Industrial Laser User 45, (2006) 27.

[4] R. Delmdahl and B. Fechner: Large-area microprocessing with excimer lasers, Appl. Phys. A101, (2010) 283.

[5] J. Xie, S. Huang, Z. Duan, Y. Shi and S. Wen: Correction of the image distortion for laser galvanometric scanning system, Opt. Laser Technol. 37, (2005) 305.

[6] M. Chen and Y. Chen: Compensating technique of field-distorting error for the CO_2 laser galvanometric scanning drilling machines, Int. J. Mach. Tool. Manuf. 47, (2007) 1114.

[7] M. Chen, Y. Chen and W. Hsiao: Correction of field distortion of laser marking systems using surface compensation function. Opt. Lasers Eng. 47, (2009) 84.

[8] F. Junfei, C. Yanbin, L. Liqun and W. Lin: Coaxial monitoring with a CMOS camera for CO2 laser welding, Adv. Mater. Dev. Sens. Imag. II, Proc. SPIE 5633, (2005) 101.

[9] J. Beersiek: A CMOS camera as a tool for process analysis not only for laser beam welding, 20th International Congress on Applications of Lasers & Electro-Optics (2001).

[10] L. Nicolosi and R. Tetzlaff: Real time control of curved laser welding processes by cellular neural networks (CNN): first results, Adv. Radio Sci. 8, (2010) 117.

[11] K. Cheol-Hee and A. Do-Chang: Coaxial monitoring of key hole during Yb:YAG laser welding, Opt. Laser Technol. 44, (2012) 1874.

[12] K. Bronowski – Opto Sonderbedarf GmbH, London Centre for Nanotechnology (LCN): TV-Microscope with Coaxial UV-Lasercoupling, Gräfelfing (2008).

[13] F. Widmer and T. VanderWert: Optical Focus Control for Precision Laser Drilling of Aircraft Engine Components, MLA 7th Edition, Adv. Manuf. Technol., (2011).

[14] MOPA-M-HP Pulsed Fiber Laser, Technical Specification Sheet, version 1.05, 2010.

[15] 2-axis deflection units, Miniscan-7 Datasheet, Raylase AG. www.raylase.de, 2013.

[16] Standard f-Theta objective S4LFT0162/126, Datasheet, Sill Optics. www.silloptics.de/, 2013

[17] Precision Stages PMT-160-DC-300-R, Technical data, Steinmeyer FMD Dresden. www.steinmeyer.com, 2013.

[18] L. Wagner: Untersuchung möglicher Strategien zur Erweiterung des Arbeitsfeldes beim Remote-Laserstrahlschneiden (2012), TU-Dresden.